A new methodology to analyze time sequences of ultrasound images

Isabelle Herlin, Nicholas Ayache

UNITÉ DE RECHERCHE
INRIA-ROCQUENCOURT

Institut National
de Recherche
en Informatique
et en Automatique

Domaine de Voluceau
Rocquencourt
B.P. 105
78153 Le Chesnay Cedex
France
Tél. (1) 39 63 55 11

Rapports de Recherche

N° 1390

Programme 4
Robotique, Image et Vision

A NEW METHODOLOGY TO ANALYZE TIME SEQUENCES OF ULTRASOUND IMAGES

Isabelle L. HERLIN
Nicholas AYACHE

Janvier 1991

Programme 4
Robotique, Image et Vision

Une nouvelle méthodologie pour l'analyse de séquences d'images échocardiographiques

A New Methodology to Analyze Time Sequences of Ultrasound Images

Isabelle L. HERLIN
Nicholas AYACHE

Février 1991

Résumé

Le fait que les données ultrasonores soient obtenues en coordonnées polaires crée une anisotropie importante de la résolution spatiale. La transformation géométrique (appelée reconstruction cartésienne), qui permet de passer des données en géométrie polaire à une représentation cartésienne est habituellement effectuée par une interpolation bilinéaire ou un algorithme de Bresenham.

Nous montrons dans cet article les limites de ces méthodes, qui ne tiennnent pas compte de la résolution variable des données et nous proposons une méthode originale qui effectue le processus de reconstruction à l'aide d'un filtrage passe-bas appliqué directement sur l'ensemble des données polaires.

Nous généralisons ensuite cette approche pour extraire les contours à différentes résolutions et nous montrons comment ils peuvent être utilisé par un logiciel de modèles déformables pour syuvre une structure physiologique au cours d'une séquence temporelle. Des résultats sont présentés sur une séquence de 24 images échographiques du coeur.

Abstract

The fact that ultrasound scan lines are acquired in polar coordinates creates an important anisotropy in spatial resolution. The geometric transformation (called scan correction) which transforms the data from a polar representation to the correct cartesian representation is usually applied through a bilinear interpolation or Bresenham's scheme.

We show in this paper the limitations of these schemes which do not account for the varying resolution of the data, and we propose an original method which consists in computing the scan-conversion with a low-pass filtering of the cartesian image applied directly to the available polar data.

We then generalize this approach to extract edges at various resolutions and show how to use these edges to track some important moving structures through a dynamic temporal sequence. This is done by combining a refined edge detection (using temporal information) with classical deformable models (snakes). We present our results on a temporal sequence of 24 ultrasound images of the beating heart.

Keywords: Image Representation, Polar to Cartesian Reconstruction, Edge Detection, Dynamic Analysis, Deformable Models, Ultrasound Images.

dynamic approach is the one by Zhang and Geiser [21], who compute temporal cooccurrences to obtain both stationary points and moving points. The temporal information has also been used to filter images obtained at the same instant of the cardiac cycle [18].

2 Acquisition of an echographic image

The purpose of this section is to present the main characteristics of echographic images which must be taken into account for an algorithmic study.

A basic imaging system, called a pulsed system, is illustrated in figure 1. When the switch is in transmit position, the pulse waveform $p(t)$ excites the transducer [12].[1] This results in propagated wavefronts in the body. Immediately following the transmission, the system switches to the receive position, using the same transducer. The pulse is attenuated when it propagates into the body. When the wavefront hits a discontinuity, a scattered wave is produced. This scattered wave is received by the transducer and the resultant signal is processed and displayed. The usual processing consists of bandpass filtering, gain control and envelope detection. The intensity of a point on an echographic image is a measure of the variation of acoustical impedance at this location.

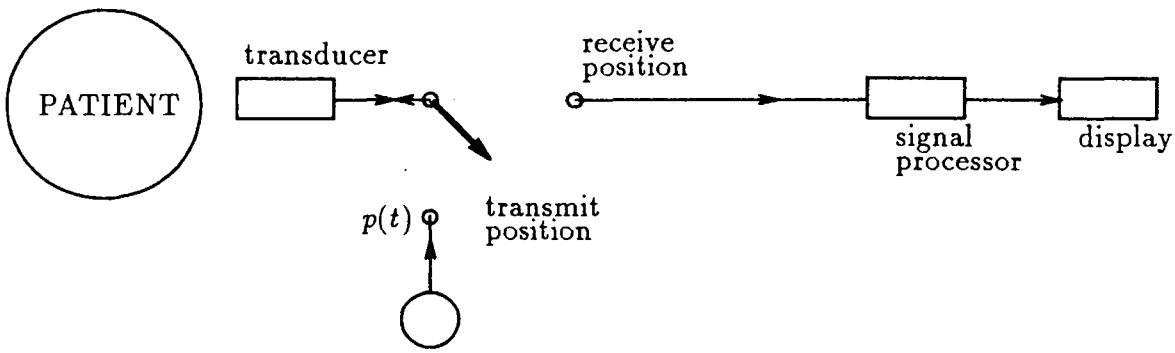

Figure 1: Elementary pulsed ultrasonic system

Post-processing of ultrasonic signal supposes that ultrasonic wavefronts propagate at constant speed. This property is quite a good approximation in the human body : the acoustical wavefronts propagate at approximately the same speed as in water (1540 m/s). When the wavefront hits a discontinuity of acoustic impedance a little part of energy (1%) is reflected towards the emitter,whereas the major part goes on through deeper structures. The attenuation of the acoustical signal is almost independent of the medium. These uniformity characteristics allow to obtain echographic images of the human body.

[1]Other types of echographs using pseudo-random code correlation are studied in the literature [15]

If only one ultrasonic beam is studied and if the pulsations are periodic in time, a M scan is obtained. These data are often used in echocardiography, because they present a good temporal resolution and allow to quantitatively measure variations of beating heart's cavities. Automatic study [19] of these data is particular because temporal resolution is much better as that of other types of echographic images. The most popular presentation of echographic results is the B scan or B mode, which is the reflectivity of a two-dimensional slice through a portion of the body. With almost all transducers, the data are obtained in polar coordinates.

The poor quality of this image is caused by two different physical phenomena.

- The speckle, due to reflections on micro tissue structures. Its probability law [20] or its textural properties [5] [13] are studied in the literature.
- The lateral width of the ultrasonic beam.

A last remark concerns the resolution of the digital ultrasonic image. There is usually an important anisotropy between the spatial resolutions (axial, lateral, azimuthal, see figure 2):

- Axial resolution corresponds to time: it is directly linked to the length of an individual echo signal and therefore directly linked to the pulse response of the probe in an emission-reception mode.
- Lateral and azimuthal resolution are associated to the spatial width of the ultrasonic beam. These resolutions are usually linked by complex relations, provided by the constructors.

3 Image representation in cartesian coordinates

We now study the geometric transformation which maps an image from a polar representation to a cartesian representation (scan correction).

The ultrasound data are described by a matrix A with N_t lines and N_r columns. N_t corresponds to the number of ultrasound beams pulsed in the body. N_r corresponds to the digitization made along each beam.

On figure 3 an echographic image, provided by a commercial echograph, is represented in polar coordinates. On figure 4 we can see the cartesian image, corresponding to these raw data.

This conversion process requires the knowledge of the following set of parameters (see figure 5) :

3.1 Conversion by nearest point or bilinear interpolation

This method is the simplest. Given M a point on the cartesian space, we want to give a grey level value to M. The cartesian coordinates of M are noted (x, y). If M is in the data acquisition cone, we note ρ and θ its new coordinates.

Let

$$l = \sqrt{(x - x_0)^2 + y^2}$$

where $(x_0, 0)$ are the cartesian coordinates of point S, vertex of the acquisition cone.
Let

$$\phi = arctg(\frac{y}{x - x_0}) - \frac{\pi - \alpha}{2}$$

One can see that:

- $l = d(M, S)$ is the euclidian distance between M and S.
- $\phi = (\overrightarrow{SE}, \overrightarrow{SM})$ is the oriented angle between vector $\overrightarrow{SE}$ and vector $\overrightarrow{SM}$ (see figure 5 for the signification of S and E).

We can define :

$$\begin{cases} \theta = \phi / \Delta_\alpha \\ \rho = l * e - \Delta_N \end{cases}$$

where :

- $\Delta_N = d * \frac{(N_r - 1)}{(D - d)}$ comes into focus because the acquisition process begins at a distance d from the skin,
- $\Delta_\alpha = \frac{\alpha}{(N_t - 1)}$ is the angular difference between two following beams,
- $e = \frac{D}{(D - d)} \frac{(N_r - 1)}{(N_y - 1)}$ performs the scale change during the reconstruction: we choose the size N_y of the cartesian image.

We note r and t the nearest integer values of ρ and θ. The algorithm gives M the grey level of point I, in the original data, with coordinates (r, t). (See figure 6).

The conversion by bilinear interpolation uses the same notations as the previous ones (see figure 6). The only change is that r and t are the integer parts of ρ and θ. We consider, on the original data, four points A, B, C, D with polar coordinates $(r, t), (r + 1, t), (r, t + 1), (r + 1, t + 1)$. The grey level of M is the weighted mean of the grey levels of the four points A, B, C, D. Weighting coefficients are the inverse of the distances between M and these four points. These distances may be calculated in cartesian space or new coordinates space.

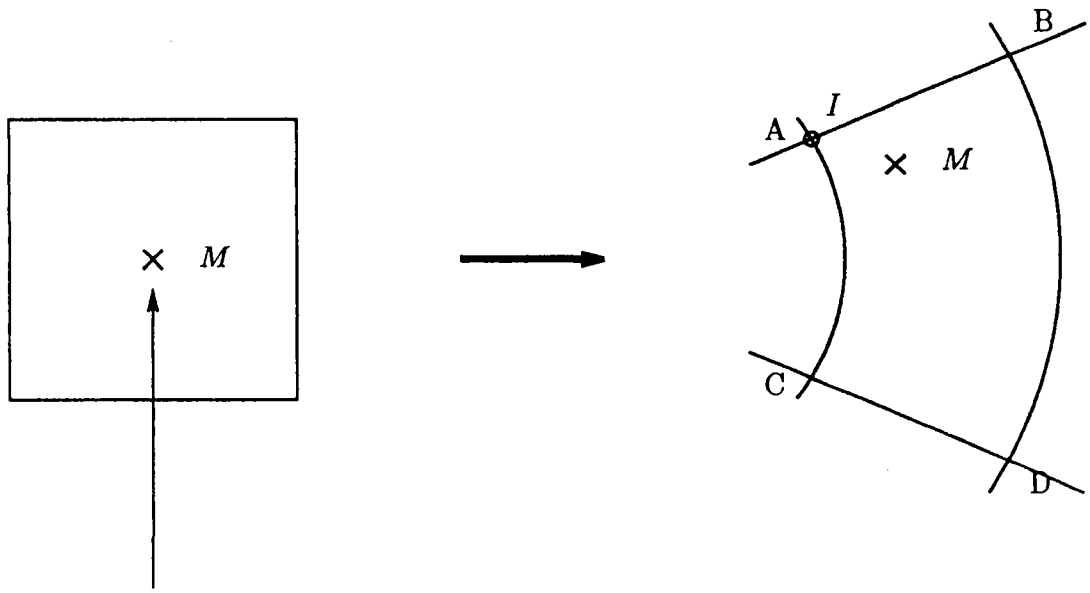

Figure 6: Reconstruction by nearest point I or bilinear interpolation between A,B,C and D.

These two algorithms are very simple to implement. Their results for image representation are acceptable, but they present some major drawbacks for posterior processing, as we show later.

Resolution of the reconstructed cartesian image is not adapted to the actual resolution of the polar ultrasonic scanning : all acquired data are not used in the area close to the skin, and interpolation corrupts the results in deep areas.

3.2 Conversion by Bresenham's algorithm

This algorithm comes from the image synthesis field [16]. A pixel is considered as a little surface and not as a simple point. To give the grey level of pixel P in the cartesian image, it is necessary to look at polar pixels that have an intersection with P. Then the grey level of P is the weighted mean of the grey levels of these polar pixels. The weighting coefficients are the surfaces of intersection (See figure 7).

The implementation may be done with the following approximation. The squared cartesian pixel is subdivided into $n \times n$ parts, denoted P_i for i between 1 and $(n \times n)$, where n is a parameter chosen by the operator. Let :

- $I(P)$ be the grey level of the cartesian pixel P. We want to choose a value for $I(P)$,
- $R(P_i)$ be the grey level of the polar pixel Q (original data), such that the barycenter

of P_i is located in Q.

We define :

$$I(P) = \frac{1}{n \times n}[\sum_{i=1}^{n \times n} R(P_i)]$$

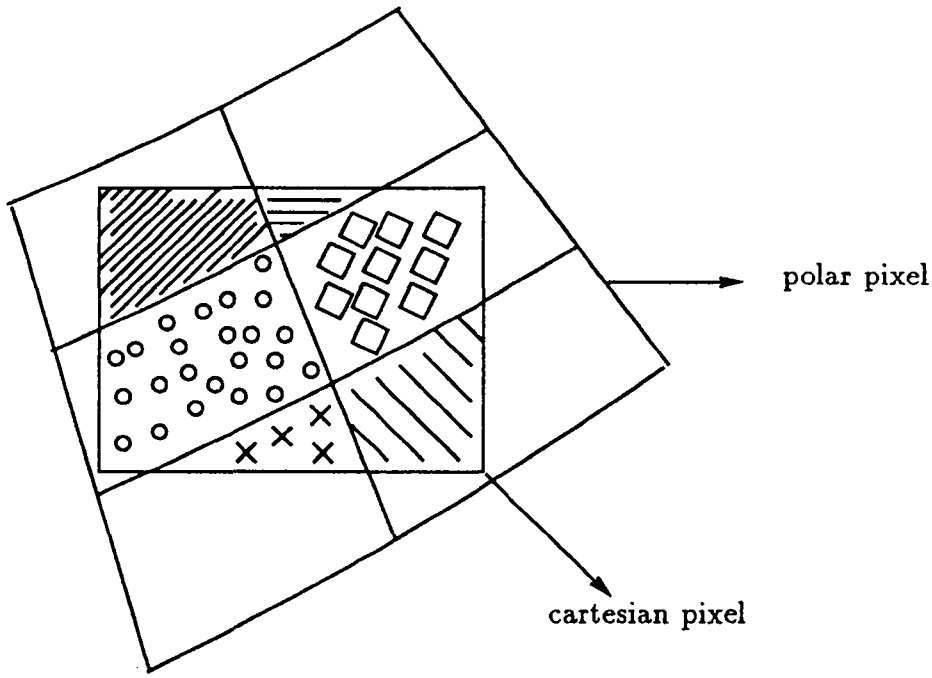

Figure 7: Conversion by Bresenham's algorithm

3.3 Conversion by direct convolution

3.3.1 Method

This is the new method we introduce [8]. We consider that $f(x,y)$ is the impulse response of a linear filter applied to the cartesian image $I(x,y)$. The resulting image $R(x,y)$, in continuous space, is given by the convolution product:

$$R(x,y) = \int_{-\infty}^{\infty}\int_{-\infty}^{\infty} f(x-u, y-v)I(u,v)dudv$$

We then apply the following change of variables :

$$\begin{cases} \theta = (\arctan(\frac{y}{x-x_0}) - (\frac{\pi-\alpha}{2})/\Delta_\alpha dT \\ \rho = (\sqrt{(x-x_0)^2+y^2}) * e - \Delta_N \end{cases}$$

where $e, \Delta_N, \Delta_\alpha$ were previously defined, to obtain the following product of convolution:

$$R(x,y) = \int_0^{2\pi} \int_0^{\infty} f(x - u(\rho,\theta), y - v(\rho,\theta)) I(\rho,\theta) \mid \mathrm{Jac}(\rho,\theta) \mid d\rho d\theta$$

where $|\mathrm{Jac}(\rho,\theta)\mid$ is the determinant of the Jacobian matrix corresponding to the following change of variables:

$$\begin{cases} x &= (\frac{\rho + \Delta_N}{e}) \cos(\theta\Delta_\alpha + \frac{\pi - \alpha}{2}) + x_0 \\ y &= (\frac{\rho + \Delta_N}{e} \sin(\theta\Delta_\alpha + \frac{\pi - \alpha}{2}) \end{cases}$$

So

$$\mid \mathrm{Jac}(\rho,\theta) \mid = \frac{(\rho + \Delta_N) * \Delta_\alpha}{e^2}$$

We have obtained an infinite and continuous product of convolution in polar coordinates, corresponding to our true data. The computer implementation requires a finite discrete summation.

Once the two-dimensional convolution filter f is chosen, we can define its finite support: a rectangular window of width $(2X + 1)$ and $(2Y + 1)$. Outside this support the absolute value of the impulse response must be lower than a chosen threshold s :

$$|f(u,v)| < s \text{ if } ((|u| \geq X) \text{ OR } (|v| \geq Y))$$

Therefore the product of convolution is limited to the domain

$$(x - X \leq u \leq x + X) \text{ AND } (y - Y \leq v \leq y + Y)$$

A sampling of the filter is also made in this domain to get a discrete summation. Filtered numerical outputs are computed at original data points locations within the continuous domain.

We obtain the following equation :

$$R(x,y) = C \sum_i f(x - u(\rho_i,\theta_i), y - v(\rho_i,\theta_i))\ I(\rho_i,\theta_i) \mid \mathrm{Jac}(\rho_i,\theta_i) \mid$$

where C is used to normalize the data and

$$\mid \mathrm{Jac}(\rho_i,\theta_i) \mid = \frac{(\rho_i + \Delta_N) * \Delta_\alpha}{e^2}$$

Therefore, $R(x,y)$ is obtained with a discrete convolution on a window $((x - X, x + X), (y - Y, y + Y))$. The difference for the raw data, or more generally for any anisotropic data, is that the sampling of the filter is not regular along x and y axis but is really adapted to

the local density of our original polar data. In this formula, one could notice that $|\mathrm{Jac}(\rho_i, \theta_i)|$ represents the surface of the polar pixel.

In practice the convolution filter $f(x,y)$ is considered separable and it is denoted by $f(x)g(y)$. Then, classical smoothing and derivation filters can be used. For the conversion by convolution on the polar data, we used the Deriche's smoothing function [6]:

$$g(x) = k_2(\alpha sin(\omega \mid x \mid) + \omega cos(\omega \mid x \mid))^{-\alpha|x|} \quad (1)$$

The conversion algorithm performs simultaneously a smoothing of the data (whose amplitude can be adjusted with α) thus producing a cartesian image with a reduced speckle. Other smoothing functions might be used.

3.4 Comparison

3.4.1 Algorithmic complexity

All three methods have been used for reconstruction of echographic images. To perform bilinear interpolation reconstruction, we need to compute an average of four grey level values at each point of the digital cartesian grid inside the data acquisition cone. If Bresenham's algorithm is used to perform reconstruction then we need to compute an average sum over n by n values inside this acquisition cone. Finally our method involves a discrete convolution of size $(2X+1)$ by $(2Y+1)$ at each point of the cone.

3.4.2 Flexibility

Our new approach is much more powerful and flexible than the previous schemes, allowing a chosen level of smoothing of the noise with an automatic adaptation to the local resolution of the image, which is not the case for bilinear interpolation or Bresenham's reconstruction.

This superiority will appear even more clearly when we compare the results of further processing like edge extraction. As we show in the next sections, we obtain much better edges in terms of detection, connectivity and smoothness, in all the parts of the image.

4 Experimental Results

This section is devoted to the results obtained for image reconstruction and further processing (edge extraction). Cartesian reconstructions of the polar image of figure 4 are shown in figure 9 (bilinear interpolation), figure 10 (Bresenham) and figure 11 (convolution with filtering parameter $\alpha = 4.0$, see equation 1). Figure 8 shows a manual sketch of the image which explains where is the sought cardiac cavity.

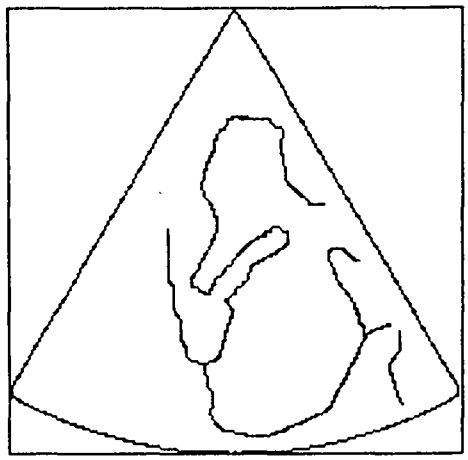

Figure 8: Manual sketch of the image

The results of the three methods may appear similar. In fact, if we now apply the Deriche's egde detector [6] to images 9,10 and 11 with exactly the same parameters, we obtain the results shown in figures 12 to 17. At this resolution, edges chains are smoother and better connected with our method, especially for the deeper structures (bottom part of the figure), but also in most parts of the image. The major drawback of our method is that we need more computing time.

For time tracking of a cardiac structure the results of classical methods are not good enough. In fact, they can be strongly improved by low-pass filtering the data. When the cartesian image is obtained by bilinear interpolation or by the Bresenham's algorithm, one must apply an *additional* filtering by convolving both the lines and columns of the obtained cartesian images. This can be done with the Deriche filter (equation 1).

On the other hand, such a smothing is obtained *within* the cartesian conversion process by applying our method (conversion by direct convolution) with the impulse response of equation 1.

Image smoothing makes boundaries more continuous as it looses some details and produces a less accurate detection. This phenomenon becomes more important as smoothing increases (i.e. as α coefficient of equation 1 becomes smaller). The difference between the images appears when we extract edges. They are extracted with exactly the same procedure as before (2-D Deriche filter with $\alpha = 0.4$), and the results are shown in figures 18 to 23. The superiority of our approach is demonstrated on this example, where the boundaries of the cavities of the heart are accurately detected, whereas the other approaches tend to miss some edges for shallow positions and to produce a less accurate detection for deeper positons.

On figures 27 to 30 we give a synthetic example showing explicitely how edges may be lost for shallow structures. One these pictures, a narrow vertical band is represented and

we can see that edge detection is not correctly performed through a bilinear interpolation followed by a smoothing, whereas it is correctly computed with our method.

Moreover if classical methods are enhanced by a smoothing, their total amount of computing time is getting more important since smoothing computation is then exactly equivalent in time to our reconstruction.

We can summarize the advantages of the reconstruction by convolution :

- One can chooze a variable level of smoothing, without the need of an extra convolution.
- Edges are better detected and more accurate, even for deep structures.
- Small details are not forgotten for shallow structures.
- computing time is less expensive.

We point out that in order to keep more details , the smoothing level is usually lower high than that one used in figures 18 to 20. On figure 24, one can see the reconstructed image through direct convolution with α=1, then the image showing the detected edges (25) and the superimposition on the original image (26). Local distorsions (due to speckle noise) may eventually become apparent for a lower spatial smoothing but they can be suppressed by a temporal smoothing as it is explained in the next section.

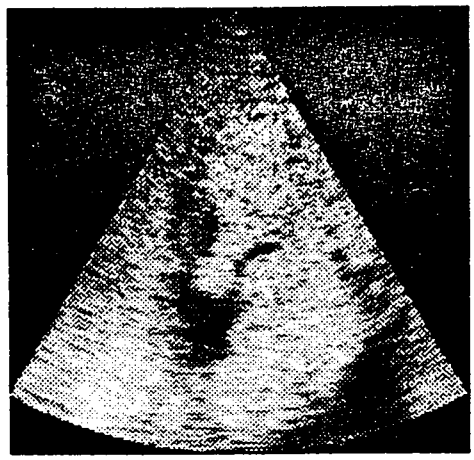

Figure 9: Reconstruction by bilinear interpolation

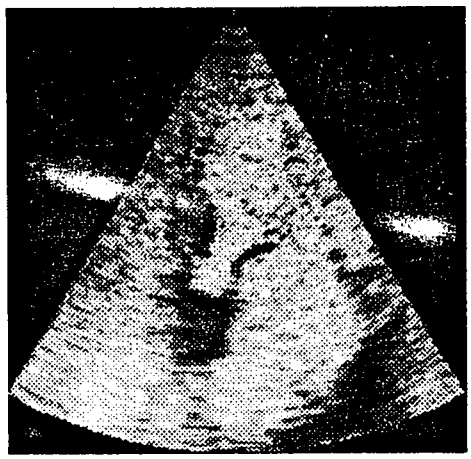

Figure 10: Reconstruction by Bresenham's algorithm.

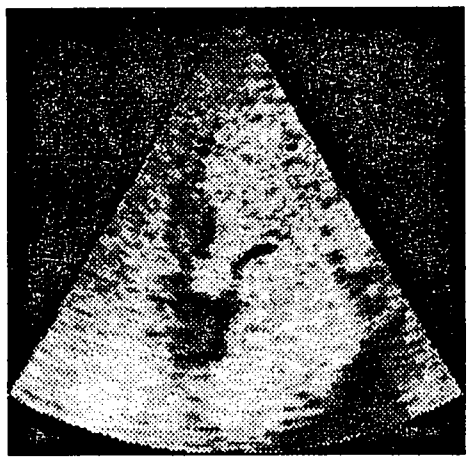

Figure 11: Reconstruction by direct convolution, α=4.0.

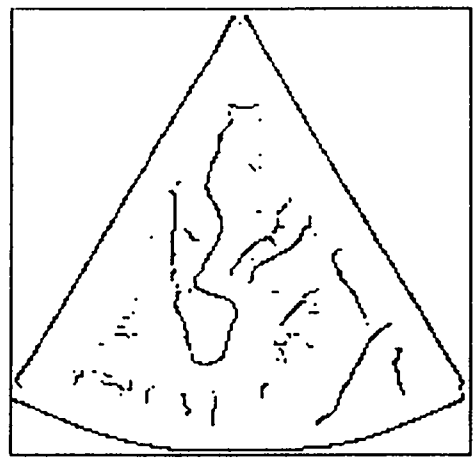

Figure 18: Edges obtained after smoothing cartesian image obtained by bilinear interpolation

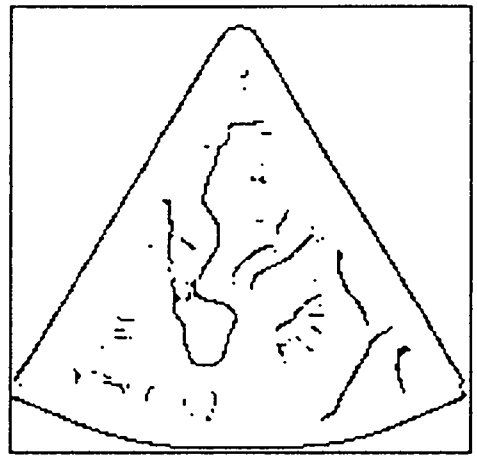

Figure 19: Edges obtained after smoothing cartesian image obtained by Bresenham's scheme

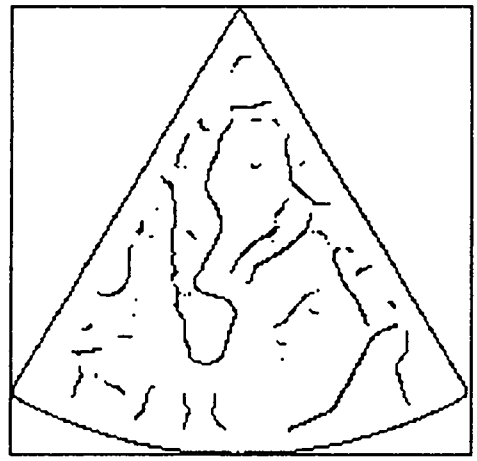

Figure 20: Edges on cartesian image obtained by convolution with α=0.4

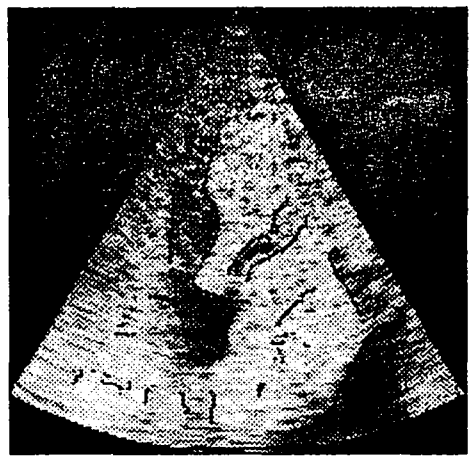

Figure 21: Edges obtained after smoothing cartesian image obtained by bilinear interpolation

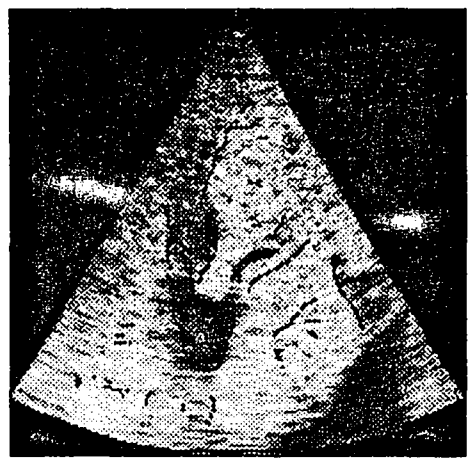

Figure 22: Edges obtained after smoothing cartesian image obtained by Bresenham's scheme

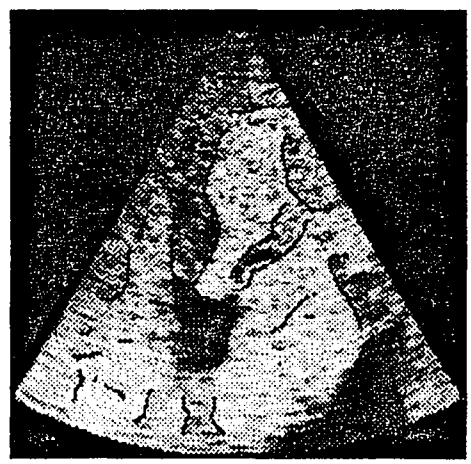

Figure 23: Edges on cartesian image obtained by convolution with α=0.4

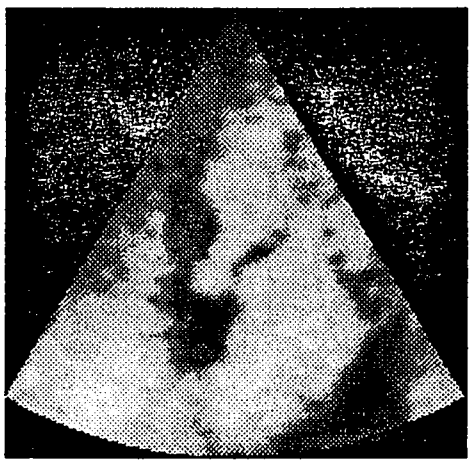

Figure 24: Reconstruction by convolution with α=1.0

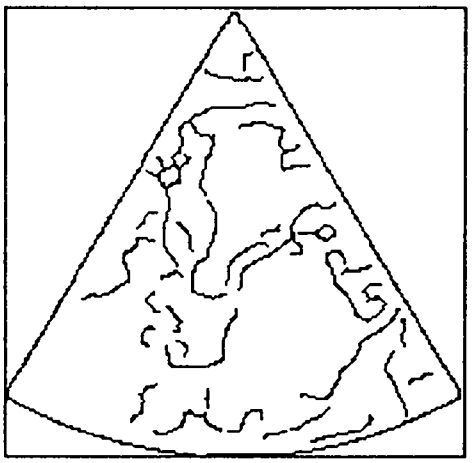

Figure 25: Edges on cartesian image obtained by convolution with α=1.0

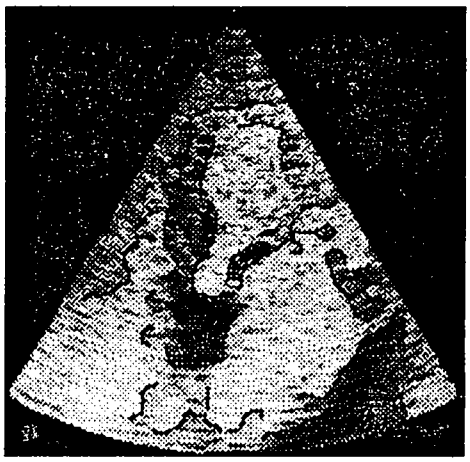

Figure 26: Superimposition of edges on cartesian image

Figure 27: Original image

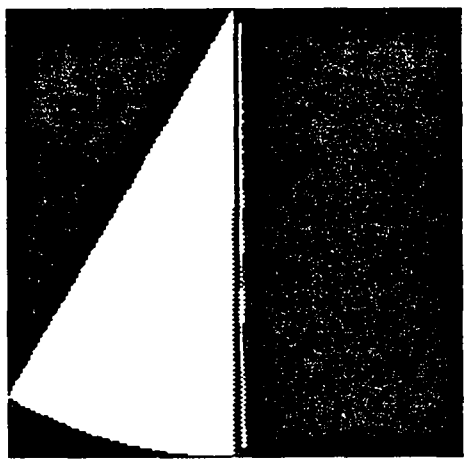

Figure 28: Reconstruction by bilinear interpolation

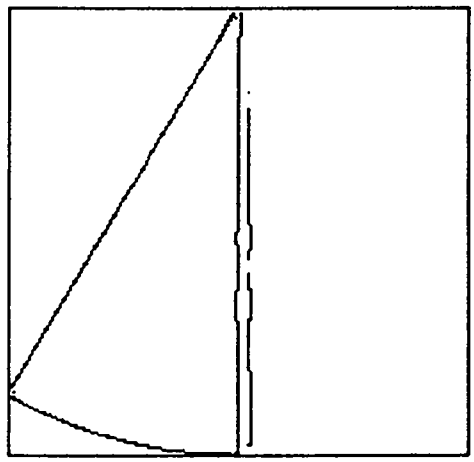

Figure 29: Edges computed on the cartesian image obtained by bilinear interpolation and smoothing (α=1.1)

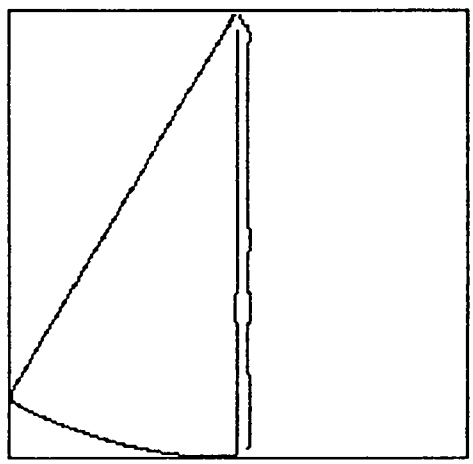

Figure 30: Edges on the cartesian image obtained by direct convolution on raw data (α=1.1)

5 Results on automatic boundary tracking

5.1 Spatio-temporal edges

For automatic boundary tracking, our goal is to use spatio-temporal approaches [14]. A time-varying edge may be represented as a surface in 3-D space, in which x and y are two spatial dimensions and t is the temporal dimension. We modify Deriche's edge detector for this goal. We note α_x, α_y and α_t the filtering parameters of the Deriche filter (cf. equation 1 for the respective dimensions x, y and t). The 2D space being homogeneous, we can choose $\alpha_x = \alpha_y$. The value of α_t is independent and must be chosen following informations about the temporal resolution. Another approach could be to generalize Deriche's detector with spatio-temporal functions as in [9]. We note G_x and G_y the two spatial components of the gradient vector and $I(x, y, t)$ the 3-dimensional grey level function. Let D be the Deriche's derivation filter and L the associated smoothing filter. The two components of the gradient vector have the following expression:

- $G_x = (D_x L_y L_t) \otimes I(x, y, t)$
- $G_y = (L_x D_y L_t) \otimes I(x, y, t)$

Each component is obtained by derivation in the associated direction and filtering in the other spatial direction and in the temporal direction. The norm of the gradient is defined by:

$$N(x, y, t) = \sqrt{G_x^2 + G_y^2}.$$

The edges are obtained as local maxima of the gradient norm in the direction of the 2D gradient vector. The temporal dimension is only used to smooth the result. This produces a significant image enhancement.

5.2 Estimation of the boundaries of the physiological structure

To obtain some crude estimation of the boundaries of physiological structures, we use mathematical morphology. The model of a cardiac cavity is very simple. this is an ovoid region with low intensity. These regions cannot be obtained by simple thresholding because of the speckle noise. The fine structures of the speckle may be easily suppressed by morphological operations:

- A first order opening eliminates the small bright structures on dark background.
- The dual operation (first order closing) suppresses the small dark structures.

After these operations, a simple thresholding gives an image C where all the cardiac cavities are represented in white. This detection can be refined by the use of higher level information. The specialist points out with the computer mouse the chosen cavity on the image. The whole cavity is then obtained by a conditional dilatation which begins at this point.

This operations usually provide a correct but inaccurate localisation of the structures boundaries. To go from this crude to an accurate localisation, we introduce finally a deformable model.

5.3 Use of a deformable model

We are using the deformable model defined by L. and I. Cohen [4]. Deformable models are mathematical entities which describe the shapes of objects appearing in images [11]. The model is applied on the image by the action of "external forces" which move and deform it from its initial position to stick it for the best to the desired attributes in the image. The crude estimation of the boundaries is deformed and attracted by local maxima of the spatio-temporal gradient, that we have precedently computed. This first application of the model permits to have precise contours in an image using a simple initial guess. It can be used in a second step to follow contours in a sequence of images at successive time steps. By following contours through time, the deformation of the object can be tracked.

5.4 Results

The first aim of this section is to present the progress that can be done on edge detection for echographic images by using the temporal information.

The principal result is that temporal smoothing permits to avoid some local distorsion on the deeper edges of the left auricle (bottom right cavity of figures 8, 31 and 32). Simultaneously, a problem may appear for the mitral valve (middle thin strycture of figures 8, 31 and 32), which is moving too fast with respect to temporal resolution. So the strategy is to use temporal smoothing only to study cavities and to apply spatial gradient to study fast moving structures like the valves.

We show in Fig. 33 the global chain of processing we have implemented for the analysis of sequences of echocardiographic images.

This chain was experimented on four different sequences obtained from two different echographs. We present a typical result of temporal tracking of an important cardiac structure, the left auricle. The sequence of ultrasound scan lines is acquired in a polar coordinate form. The part of sequence that we have studied contains 24 images. We show the temporal tracking of the left auricle.

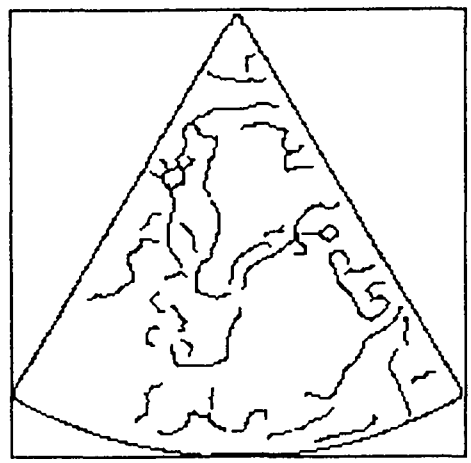

Figure 31: No temporal smoothing of edges on the cartesian image obtained by direct convolution, $\alpha_x = \alpha_y = 1$.

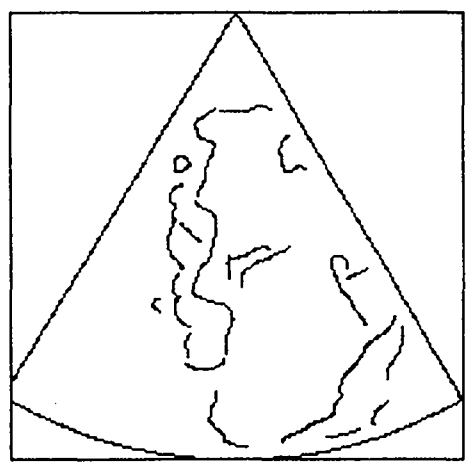

Figure 32: Temporal smoothing of edges on the cartesian image obtained by direct convolution, $\alpha_x = \alpha_y = 1$, $\alpha_t = 1.5$

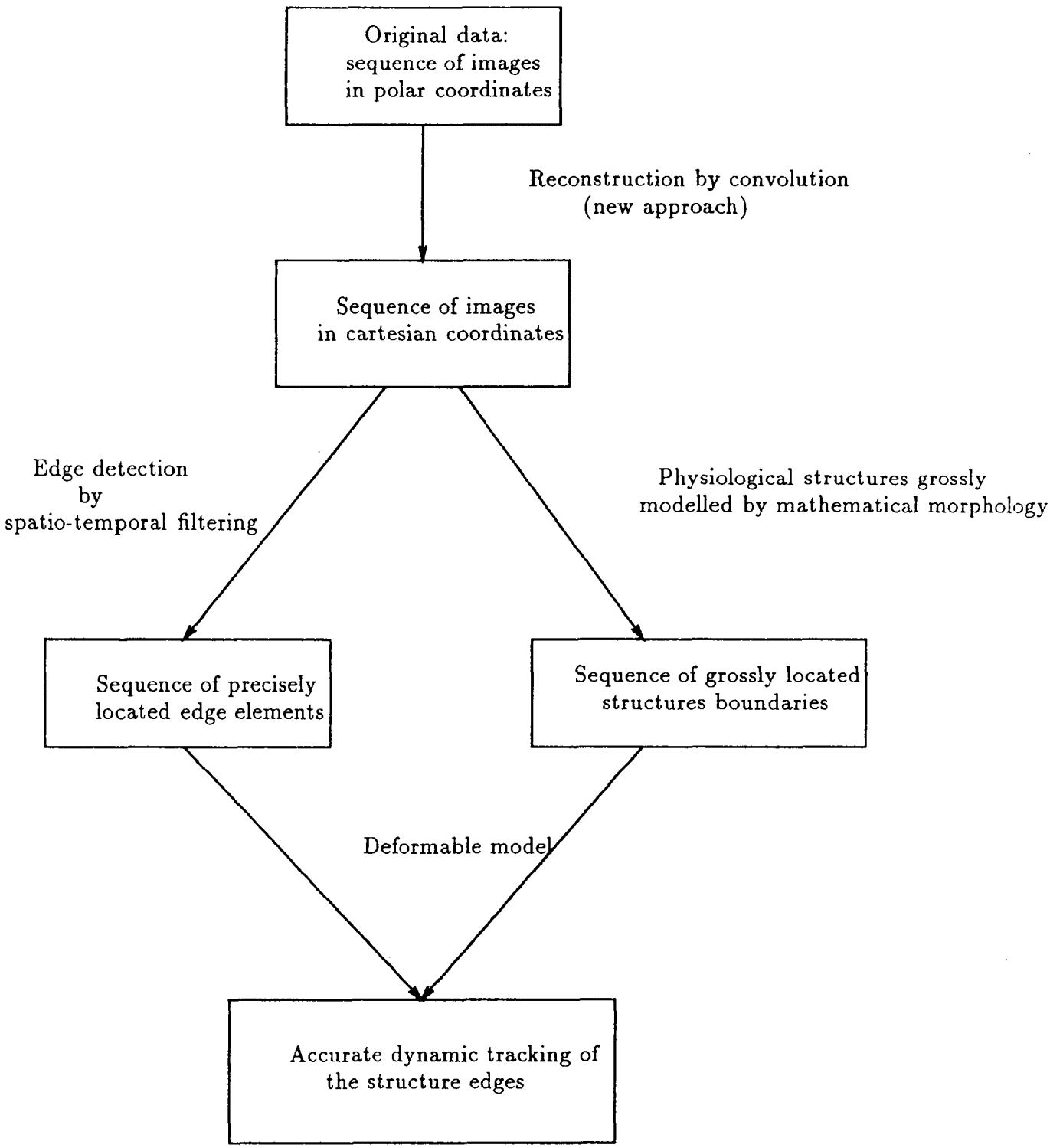

Figure 33: Description of the global chain

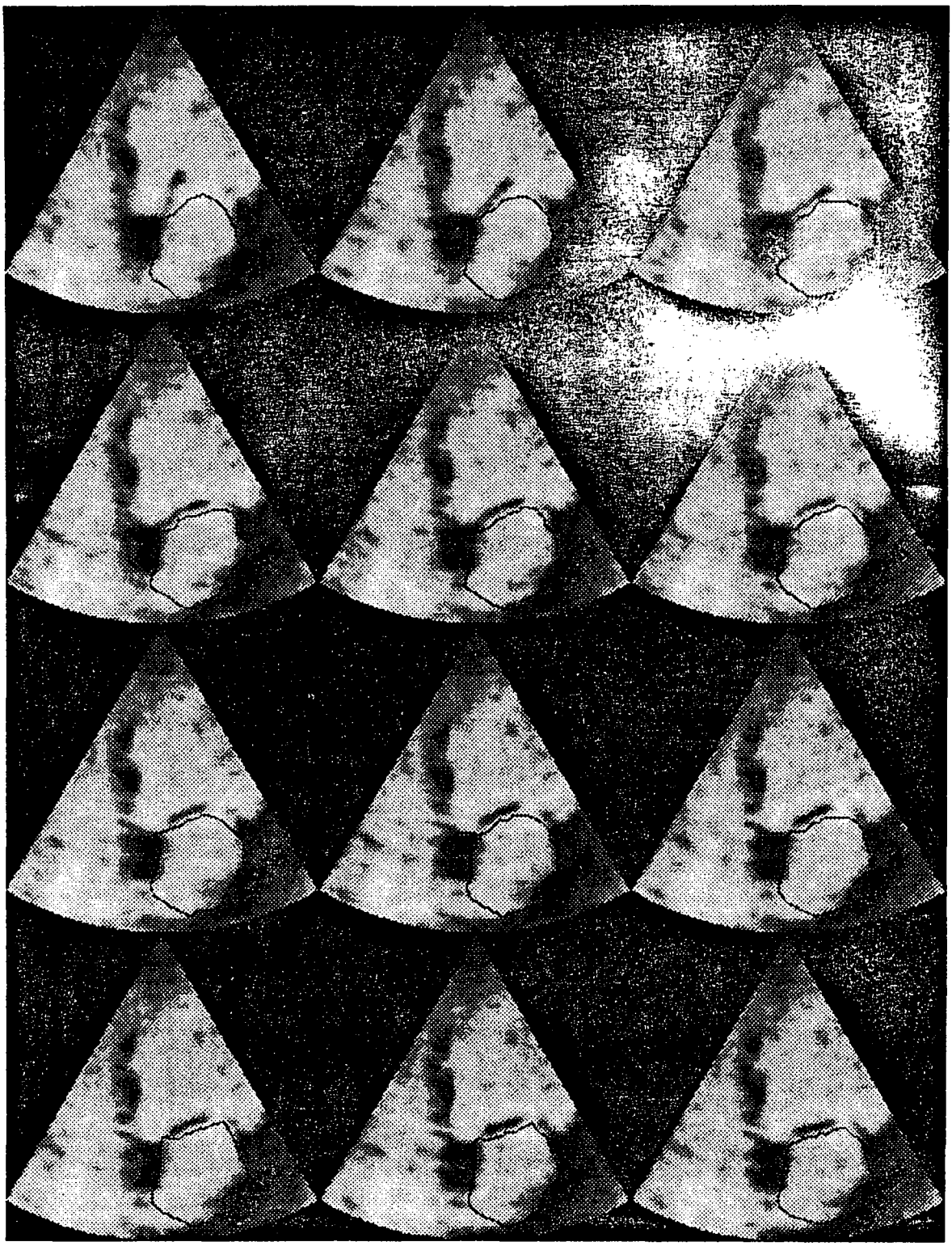

Figure 34: Temporal sequence of cartesian image, first part

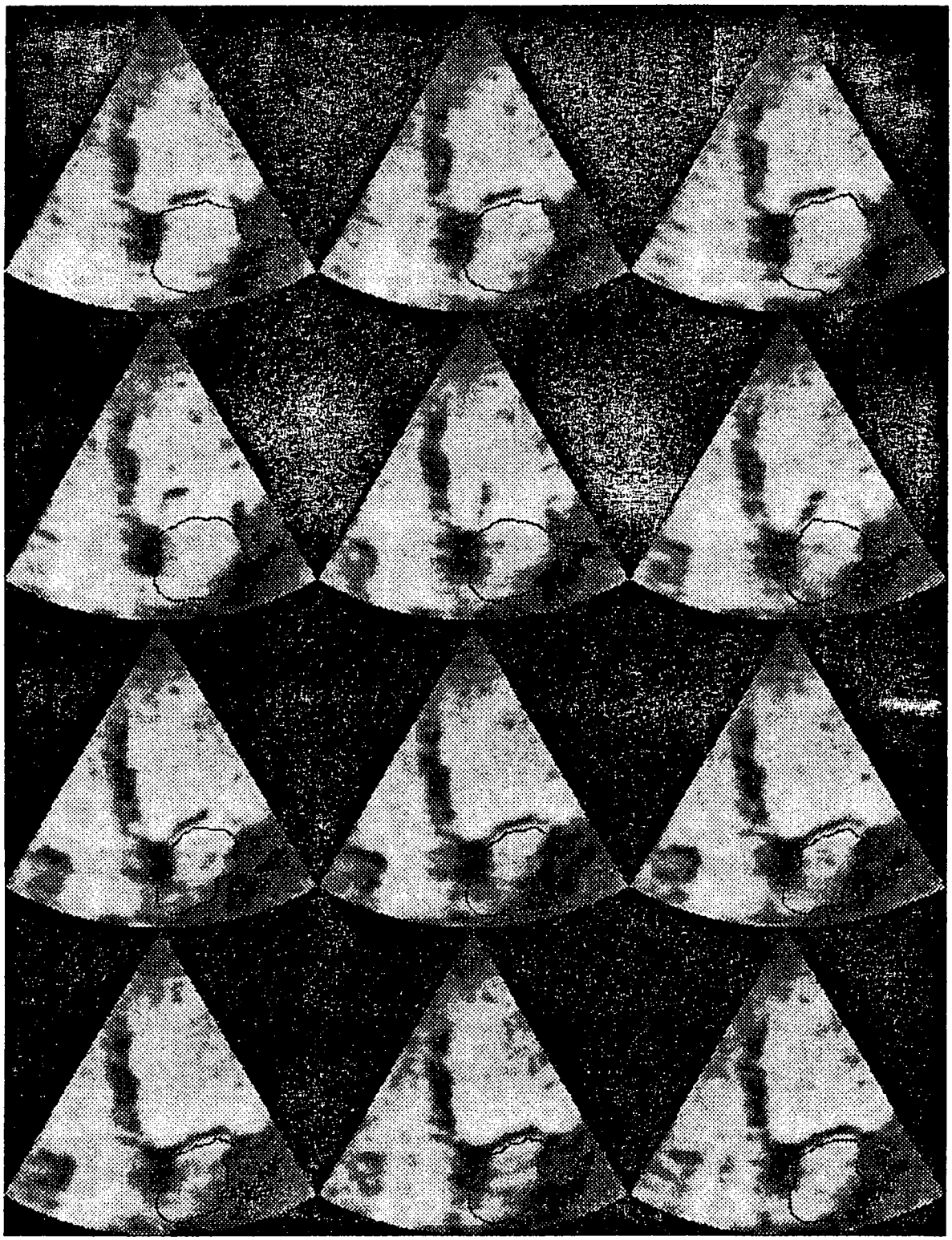

Figure 35: Temporal following of the left auricle,second part

6 Conclusions

We showed in this paper the importance of using an appropriate conversion method when dealing with images produced in polar coordinates. We showed that the classically used algorithms of bilinear interpolation and Bresenham produce images which are not well suited for further processing like smoothing and edge detection.

We introduced a new method which computes both the conversion and a convolution of the polar data with a smoothing filter. This approach is more flexible than the previous ones because it allows a variable level of smoothing adapted to the actual resolution of the original data. This is not the case when an additional smoothing is required after a conversion by the other algorithms.

We showed the enhancement produced on edge detection by our approach, where smoothing and conversion are obtained at the cost of a single product of convolution whereas other algorithms require an additional (often costly) specific conversion algorithm. We also demonstrated the effectiveness of combining a temporal smoothing in addition to the spatial one, to better characterize slowly varying edges.

Finally, we demonstrated the effectiveness of our approach by solving a complete application. We use morphological operators to initialize a deformable model in the first image of a time sequence. Then we apply our edge detector and we let the deformable model converge toward the detected edges. Using the solution as an initialization in the following image, we can track the left auricle boundary in a sequence of 24 images.

Our future research will concentrate on the generalization of the edge detector applied to 3-D ultrasound images produced in sherical coordinages.

7 Acknowledgements

We gratefully acknowledge Gabriel Pelle (INSERM, CHU Henri MONDOR, FRANCE) for providing the data and for helpful discussions. We also acknowledge R. Vojak who pionneeried this work, L. and I. Cohen who provided their snakes software.

This work was partially supported by MATRA Espace: contract 189D3240021120012.

References

[1] AIM-89. Avanced informatics in medicine in europe, 1989. Preliminary call for proposals.

[2] N. Ayache, J.D. Boissonnat, L. Cohen, B. Geiger, J. Levy-Vehel, O. Monga, and P. Sander. Steps toward the automatic interpretation of 3-D images. In H. Fuchs K. Hohne and S. Pizer, editors, *3D Imaging in Medicine*, pages 107–120. NATO ASI Series, Springer-Verlag, 1990.

[3] A.J. Buda, E.J. Delp, J.M. Meyer, J.M. Jenkins, D.N. Smith, F.L. Bookstein, and B. Pitt. Automatic computer processing of digital 2-dimensional echocardiograms. In *Amer. J. Cardiol.*, volume 51, pages 383–389, 1983.

[4] L.D. Cohen and I. Cohen. A finite element method applied to new active contour models and 3D reconstruction from cross sections. In *Proceedings of the International Conference on Computer Vision*, Osaka, Japan, December 1990.

[5] A. Corenthin, J. Lemoine, E. Petit, P. Provent, P. Bunel, and M. Gaudaire. Méthode de classification supervisée de textures. Application à la segmentation du myocarde sur des images échocardiographiques bidimensionnelles. Technical report, Laboratoire de génie électrique de Créteil, 1990.

[6] R. Deriche. Using Canny's criteria to derive a recursively implemented optimal edge detector. *International Journal of Computer Vision*, 1 (2), May 1987.

[7] F. Faure, J.P. Gambotto, G. Montserrat, and F. Patat. Space medical facility study. Technical report, ESA, 1988. final report, 6961/86/NL/PB.

[8] I. Herlin and N. Ayache. A new methodology to analyze time sequences of ultrasound images. Technical report, INRIA, 1991.

[9] T. Hwang and J.J. Clark. A spatio-temporal generalization of Canny's edge detector. In *10th International Conference on Pattern Recognition*, Atlantic City, New Jersey, USA, June 1990.

[10] J.M. Jenkins, O. Qian, M. Besozzi, E.J. Delp, and A.J. Buda. Computer processing of echocardiographic images for automated edge detection of left ventricular boundaries. In *Computers in Cardiology*, volume 8, 1981.

[11] Michael Kass, Andrew Witkin, and Demetri Terzopoulos. Snakes: Active contour models. In *Proceedings of the First International Conference on Computer Vision*, pages 259–268, London, June 1987.

[12] A. Macovski. *Medical Imaging Systems.* Prentice Hall, 1983.

[13] J. Meunier, M. Bertrand, and G. Mailloux. Speckle tracking in echography of the myocardium: a model study. In *Conference on biomedical technologies*, 1988.

[14] O. Monga and R. Deriche. 3D edge detection using recursive filtering: application to scanner images. Technical Report 930, INRIA, November 1988.

[15] V.L. Newhouse. *Progress in Medical Imaging*. Springer Verlag, 1988.

[16] D.F. Rogers. *Procedural Elements for Computer Graphics*. McGraw-Hill Book Company, 1985.

[17] T. Taxt, A. Lundervold, and B. Angelsen. Noise reduction and segmentation in time-varying ultrasound images. In *10th International Conference on Pattern Recognition*, Atlantic City, New Jersey, USA, June 1990.

[18] M. Unser, L. Dong, G. Pelle, P. Brun, and M. Eden. Restoration on echocardiagrams using time warping and periodic averaging on a normalized time scale. In *Medical Imaging*, number III, 1989. January 29 – February 3, Newport Beach.

[19] M. Unser, G. Pelle, P. Brun, and M. Eden. Automated extraction of serial myocardial borders form M-mode echocardiograms. In *IEEE Transactions on Medical Imaging*, volume 8, March 1989.

[20] R.F. Wagner, S.W. Smith, J.M. Sandrik, and Lopez H. Statistics of speckle in ultrasound B-scans. In *IEEE Trans. on sonics and ultrasonics*, number 30, pages 156–163, 1983.

[21] L.F. Zhang and E.A. Geiser. An approach to optimal threshold selection on a sequence of two-dimensional echocardiographic images. In *IEEE Transactions on Biomedical Engineering*, volume BMB 29, August 1982.

Imprimé en France
par

ISSN 0249-6399